LETTERS

Direct observation of electron dynamics in the attosecond domain

A. Föhlisch[1], P. Feulner[2], F. Hennies[1], A. Fink[2], D. Menzel[2], D. Sanchez-Portal[3], P. M. Echenique[3] & W. Wurth[1]

Dynamical processes are commonly investigated using laser pump–probe experiments, with a pump pulse exciting the system of interest and a second probe pulse tracking its temporal evolution as a function of the delay between the pulses[1–6]. Because the time resolution attainable in such experiments depends on the temporal definition of the laser pulses, pulse compression to 200 attoseconds (1 as = 10^{-18} s) is a promising recent development. These ultrafast pulses have been fully characterized[7], and used to directly measure light waves[8] and electronic relaxation in free atoms[2–4]. But attosecond pulses can only be realized in the extreme ultraviolet and X-ray regime; in contrast, the optical laser pulses typically used for experiments on complex systems last several femtoseconds (1 fs = 10^{-15} s)[1,5,6]. Here we monitor the dynamics of ultrafast electron transfer—a process important in photo- and electrochemistry and used in solid-state solar cells, molecular electronics and single-electron devices—on attosecond timescales using core-hole spectroscopy. We push the method, which uses the lifetime of a core electron hole as an internal reference clock for following dynamic processes[9–19], into the attosecond regime by focusing on short-lived holes with initial and final states in the same electronic shell. This allows us to show that electron transfer from an adsorbed sulphur atom to a ruthenium surface proceeds in about 320 as.

When studying electron transfer processes in complex systems, it is of equal importance to address the temporal evolution of the electron wave packet and the question of which atomic centre an electron is localized at before charge transfer to the substrate occurs. This atom specific information cannot be provided in pump–probe experiments in the spectral regime of optical transitions. By adapting an element specific synchrotron based soft X-ray spectroscopy method, namely core-hole clock spectroscopy, we can effectively determine on an attosecond timescale electron transfer dynamics originating from an atomically localized state by making use of extremely fast Coster–Kronig decay processes of core-excited states.

The principle of core-hole clock spectroscopy is to take the core-hole lifetime τ as an internal reference clock for the temporal evolution of a dynamic process under investigation[9–19]. To study charge transfer on the timescale of τ, the dynamics of an electron resonantly excited into an unoccupied state from an atomically localized adsorbate core level (Fig. 1a) is monitored through the autoionization process that accompanies the core-hole decay (Fig. 1b and c). If the initially excited core electron remains in an atomically localized resonance, a linear relation between the energies of the incoming photon and of the outgoing electron in the autoionization is observed (Fig. 1b). This is the so-called Raman autoionization channel at constant binding energy (*l*). In contrast, if the initial

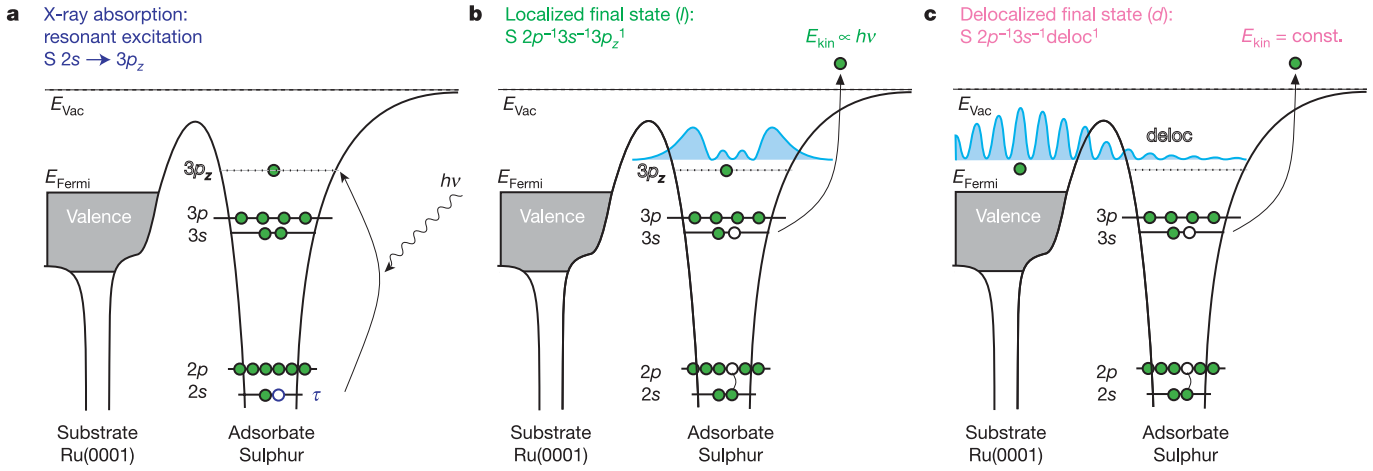

Figure 1 | Core-hole clock spectroscopy—schematic overview. a, Initially, a core electron is promoted by resonant excitation from the S 2*s* level into a bound resonance localized at an adsorbed sulphur atom ($S\,2s^{-1}3p_z^1$) on ruthenium c(4 × 2)S/Ru(0001) with a core-hole lifetime $\tau = 0.5$ fs. In the autoionization decay processes, Coster–Kronig decay of the S 2*s* core hole takes place in the presence of this electron, the so-called 'spectator' electron, leading to two different final states. **b**, Localized final state $S\,2p^{-1}3s^{-1}3p_z^1$: state *l*. The initially excited electron is still localized at the sulphur atom. **c**, Delocalized final state $S\,2p^{-1}3s^{-1}\mathrm{deloc}^1$: state *d*. The initially excited electron has already left the localized resonance. E_{vac}, vacuum energy; E_{Fermi}, Fermi energy; E_{kin}, kinetic energy.

[1]Institut für Experimentalphysik, Universität Hamburg, Luruper Chaussee 149, D-22761 Hamburg, Germany. [2]Physik Department E20, Technische Universität München, D-85747 Garching, Germany. [3]Centro Mixto CSIC-UPV/EHU "Unidad de Física de Materiales", Donostia International Physics Center (DIPC), and Departamento de Física de Materiales, Universidad del País Vasco, Apdo. 1072, 20080 Donostia-San Sebastián, Spain.

excitation involves an electronic state delocalized over many atomic centres (that is, the excited atomic resonance is coupled to a continuum), we obtain independently of the incident photon energy autoionization at constant kinetic electron energy (Fig. 1c). This is the charge transfer channel of autoionization (d). Owing to this different dispersive behaviour, the Raman (l) and charge transfer (d) channels of autoionization can be spectroscopically separated (Fig. 2a), and the ratio of Raman to charge transfer intensity is related to the degree of atomic localization in the excited state on the timescale τ of the core-hole decay. This can be translated into a dynamic picture of an electron residence time, or alternatively as the charge transfer time, τ_{CT}, of electron hopping to the substrate. As spectral intensities are compared, the $\sqrt{N}$ uncertainty (where N is the number of events) allows a statistically significant analysis only as long as the intensities of the spectroscopic channels are less than one order of magnitude apart. Thus a temporal range of charge transfer times between $0.1\tau \leq \tau_{CT} \leq 10\tau$ becomes accessible. The typical core-hole lifetimes of inner shell vacancies lie at oxygen KLL ($\tau = 4$ fs; ref. 20), nitrogen KLL ($\tau = 5$ fs; ref. 20), carbon KLL ($\tau = 6$ fs; ref. 20), and argon $L_3M_{4/5}M_{4/5}$ ($\tau = 6$ fs; refs 13, 18). We note that the core-hole lifetimes depend only weakly on the chemical environment. In a comparison between atomic and molecular systems, variations of the order of roughly 20% have been observed[20].

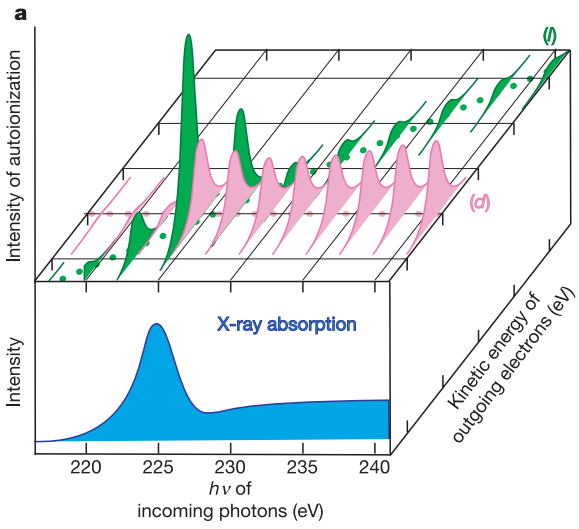

Figure 2 | Core-hole clock spectroscopy—the spectroscopic signatures. **a**, Diagram of the spectroscopic autoionization signatures leading to a localized final state (l) with linear dispersion and a delocalized final state (d) at constant kinetic energy, and their relation to resonant excitation by X-ray absorption. **b**, Experimental sulphur $L_1L_{2/3}M_{1/2/3}$ Coster–Kronig autoionization spectra of c(4 × 2)S/Ru(0001) as a function of incident photon energy.

To access dynamic processes in the attosecond range reliably, shorter core-hole lifetimes are required. Our approach is to perform attosecond charge transfer core-hole clock spectroscopy in the soft X-ray region by monitoring Coster–Kronig autoionization channels

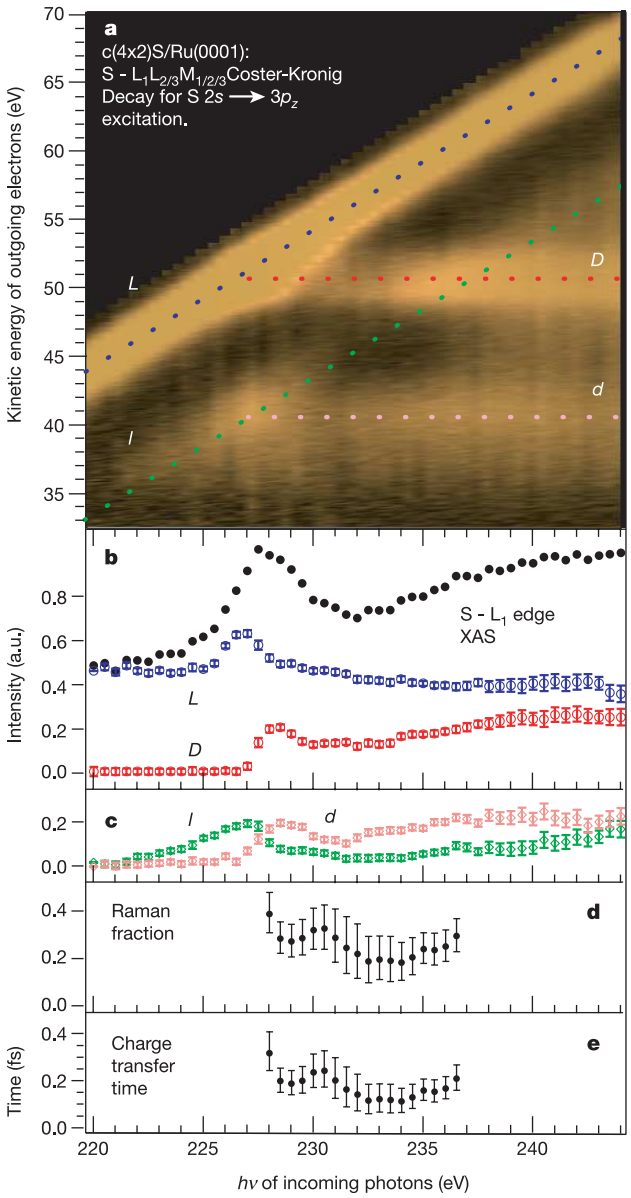

Figure 3 | Quantitative charge transfer analysis of sulphur $L_1L_{2/3}M_{1/2/3}$ Coster–Kronig autoionization spectra of c(4 × 2)S/Ru(0001) as a function of photon energy. **a**, Experimental intensities as a function of incoming photon energy and kinetic energy of the outgoing electrons. Lighter colours correspond to higher autoionization intensity. Shown are Raman channels with linear dispersion for localized final states L ($2p^{-1}3p^{-1}3p_z^1$) at 170.7 eV binding energy and l ($2p^{-1}3s^{-1}3p_z^1$) at 181.7 eV binding energy, and charge transfer channels with delocalized final states D ($2p^{-1}3p^{-1}\mathrm{deloc}^1$) at 50.8 eV kinetic energy and d ($2p^{-1}3s^{-1}\mathrm{deloc}^1$) at 40.6 eV kinetic energy. **b**, Sum of spectral intensities representing the S-L_1 edge X-ray absorption spectrum. Also shown are separate intensities of the spectral channels (L, D) from curve fitting with lorentzians of 3.3 eV FWHM. Error bars show the standard deviation of each fit. **c**, Separate intensities of the spectral channels (l, d) from curve fitting with lorentzians of 3.3 eV FWHM. Error bars show the standard deviation of each fit. **d**, Raman fraction $f = l/(l + d)$ as a function of photon energy. Error bars are derived from the standard deviation of the fits (see **c**). **e**, Charge transfer time obtained from the Raman fraction as $\tau_{CT} = \tau f/(1 - f)$ and the S 2s core-hole lifetime $\tau = 0.5$ fs. Error bars are derived from the standard deviation of the fits (see **c**).

with attosecond core-hole lifetimes. Here the initial and final state vacancies are in the same electronic shell (same principal quantum number n); the probability for these transitions is higher and the corresponding core-hole lifetimes shorter than in the case of decay processes involving different values of n.

With the c(4 × 2)-S/Ru(0001) surface[21,22], we obtained the S $L_1L_{2/3}M_{1/2/3}$ Coster–Kronig autoionization spectra shown in Fig. 2b as a function of the incoming photon energy $h\nu$ tuned across the S $2s^{-1}3p_z^1$ core level resonance at $h\nu = 227.5$ eV. On resonance, the excited electron's energy lies 1.68 ± 0.1 eV above the Fermi level. We observe resonant enhancement and branching of decay channels at this absorption resonance. The data are converted to a colour-coded plot in Fig. 3a, where higher intensity corresponds to lighter colour. We can directly discern spectral features (l, L) at constant binding energy, which branch into charge transfer spectral features (d, D) with constant kinetic energy. Let us assign the spectral features: starting from the electronic ground state (GS), the S $2s^{-1}3p_z^1$ core-excited state can autoionize through Coster–Kronig channels with and without participation of the excited electron ('participator' and 'spectator' channels, respectively). The participator channel, involving the core-excited $3p_z^1$ in the decay, leads to the spin–orbit split $2p^{-1}$ final state, identical to the main lines of photoionization, with 161.5 eV ($2p_{3/2}^{-1}$) and 162.6 eV ($2p_{1/2}^{-1}$) binding energy. Its spectral features lie outside the range of Figs 2b and 3a.

$$GS \xrightarrow{\text{Core-excitation}} 2s^{-1}3p_z^1 \xrightarrow{\text{Participator-decay}} 2p^{-1}$$
$$GS \xrightarrow{\text{Photoionization}} 2p^{-1}$$

The spectral features shown in Figs 2b and 3a are thus associated with spectator channels, in particular the $2p^{-1}3s^{-1}3p_z^1$ (l) and $2p^{-1}3p^{-1}3p_z^1$ (L) final states at 181.7 eV and 170.7 eV binding energy, respectively.

$$GS \xrightarrow{\text{Core-excitation}} 2s^{-1}3p_z^1 \xrightarrow[\text{Spectator-decay}]{} \overbrace{2p^{-1}3s^{-1}3p_z^1}^{l}$$
$$2s^{-1}3p_z^1 \xrightarrow[\text{Spectator-decay}]{} \underbrace{2p^{-1}3p^{-1}3p_z^1}_{L} \xleftarrow{\text{Shake-up photoionization}} GS$$

The $2p^{-1}3s^{-1}3p_z^1$ final state l can only be reached via autoionization, whereas the $2p^{-1}3p^{-1}3p_z^1$ final state L can in addition be reached as a photoionization satellite, obeying the monopole selection rule of photoionization shake-ups. Thus, L is present at all photon energies, whereas l is a pure autoionization feature observed only when a core hole has been present. We therefore base all further analysis on the autoionization channel l ($2p^{-1}3s^{-1}3p_z^1$) and the related charge transfer feature d ($2p^{-1}3s^{-1}deloc^1$), which branches off at 40.6 eV constant kinetic energy. The final states l and d are shown schematically in Fig. 1b and c.

To quantify the relative strength of the Raman (l) and charge transfer (d) channels, we performed a curve fit of the spectra at all photon energies with fixed line shapes, where each channel was described phenomenologically by a lorentzian of 3.3 eV full-width at half-maximum (FWHM), and only the intensities were varied. The charge transfer peaks (D, d) were kept at constant kinetic energy and the Raman peaks (L, l) at constant binding energy with varied photon energy. In Fig. 3b and c, these four contributions (D, L, d, l) and the standard deviation of the fit at each photon energy are shown together with their sum. The latter yields the S-L_1 edge X-ray absorption spectrum (XAS) (Fig. 3b) with 3 eV FWHM dominated by the S2 s core-hole lifetime of $\tau = 0.5$ fs (ref. 23). From this fit, as a function of photon energy, the relative strength of the Raman contribution expressed as the Raman fraction $f = l/(l + d)$ and the charge transfer time $\tau_{CT} = \tau f/(1 - f)$ using the S 2s core-hole life time ($\tau = 0.5$ fs) is derived and displayed in Fig. 3d and e, respectively.

For photon energies below the S $2s^{-1}3p_z^1$ absorption resonance ($h\nu = 227.5$ eV), we observe intensity in the Raman channel l only, as charge transfer below threshold is energetically forbidden, equivalent to an infinitely long charge transfer time. Just above the S $2s^{-1}3p_z^1$ resonance at $h\nu = 228$ eV, we determine $\tau_{CT} = 0.32 \pm 0.09$ fs. For higher photon energies, shorter charge transfer times down to 0.11 ± 0.06 fs at $h\nu = 234$ eV are found. An energy dependence of the electron transfer time has been observed before[15,18]. This energy dependence is most probably due to the detailed nature of the projected band structure of the substrate, and thus the number and character of the final states available, as well as their overlap with the initial adsorbate state.

We have compared our experimental results with first-principles computations of the charge-transfer dynamics in the c(4 × 2)S/Ru(0001) system. The initial electron wave packet is constructed as a linear combination of the S 3p orbitals projected onto the unoccupied bands of the combined system, that is, the Ru substrate with the adsorbed sulphur atoms, at the resonance energy. We find that the excitation into a resonance with predominantly $3p_z$ character yields a charge transfer time of 0.63 ± 0.15 fs (Fig. 4a). This corresponds to the state that is excited in the experiment. In comparing experiment to theory, the theoretical time constant confirms that the charge transfer process takes place well below a femtosecond timescale. In particular, the agreement with the experimental value of 0.32 ± 0.09 fs is very satisfactory, taking into account that the core vacancy is not described explicitly in the theoretical ground state calculation; and the theoretical resonance position at ~2 eV above the Fermi level is shifted relative to the experimental absorption resonance, which is at 1.68 ± 0.1 eV above the Fermi level. Furthermore, theory predicts a detailed dependence of the charge transfer time on the symmetry of the initial excited state,

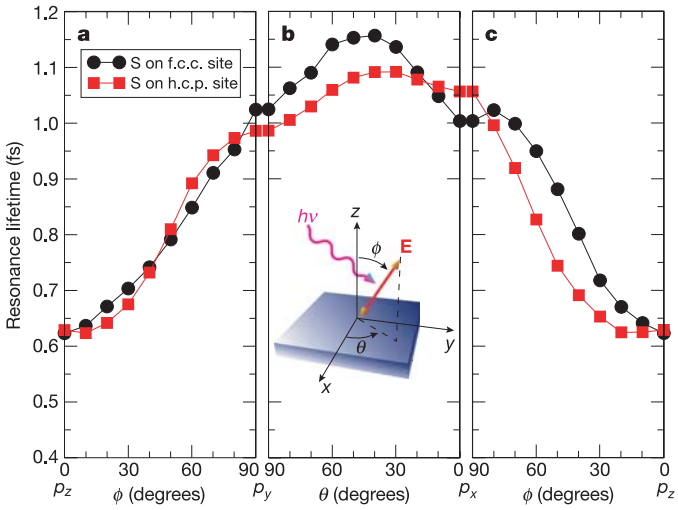

Figure 4 | Theoretical charge transfer time for S in f.c.c. and h.c.p. hollow sites computed as S 3p resonance lifetime. Theory predicts a strong dependence of the charge transfer time on the symmetry of the initial wave packet, which translates to a strong dependence on the light polarization. The coordinates x, y, z shown in the diagram in **b** correspond to the crystallographic directions [100], [010], [001]. The circles and squares correspond respectively to sulphur atoms in f.c.c. and h.c.p. sites of the surface. **a**, Resonance lifetime as a function of the angle ϕ of the electric field vector with respect to the surface normal in the y–z plane. Polarization of the synchrotron light along the z axis ($\phi = 0$, the experimental geometry) produces an initial excited state with p_z symmetry. **b**, Resonance lifetime as a function of the angle θ of the electric field vector with respect to the x axis in the x–y plane. In this geometry, p_x and p_y symmetries and combinations of them would be obtained with in-plane polarization. **c**, Resonance lifetime as a function of the angle ϕ of the electric field vector with respect to the surface normal in the x–z plane.

which is summarized in Fig. 4. For excitation into $3p_x$ or $3p_y$-like resonances (in plane) (Fig. 4b) with a smaller overlap to the substrate, a significantly larger charge transfer time of up to 1.15 ± 0.15 fs is calculated. This theoretical result indicates that different polarizations of the light favour different initial excited states, with different symmetries and overlaps with the states of the substrate, thus leading to different transfer times.

The demonstration that soft X-ray spectroscopy can be used as a tool to study the motion of electrons on attosecond timescales opens a possible way to interesting new research areas. Potentially the method is suited to the investigation of electron transfer in complex molecular systems. In such investigations, the ability to excite individual atomic centres (even atoms of the same element in chemically different environments) by exploiting core level shifts should be of particular importance. A second future application could be the investigation of spin-dependent electron transfer processes, which are important in spintronics. Here core level excitation using circularly polarized light could be used to create spin-polarized excitations.

METHODS

Experiments. The experiments were performed at beamline I311, MAX-lab in Lund, Sweden. At 5×10^{-11} torr base pressure, a clean Ru(0001) surface was prepared by cycles of Ar^{+}-ion sputtering, oxygen-exposure and annealing. The c(4 × 2)S/Ru(0001) surface, with sulphur atoms chemisorbed in hexagonal close packed (h.c.p.) and face-centred cubic (f.c.c.) hollow sites[21,22], was prepared by dissociative adsorption of 400 Langmuir H_2S (1 Langmuir $= 10^{-6}$ torr s) at 550 K and annealing to 850 K. The surface quality was checked by core electron spectroscopy (XPS) and low-energy electron diffraction (LEED). At 7° grazing incidence, the electric field vector of the incident radiation was 7° off the surface normal, exciting preferentially into the S $3p_z$ orbital oriented normal to the surface. The electron spectrometer (Scienta SES 200) was in the polarization plane at 45° to the incident radiation. Narrow bandwidth excitation and high spectral resolution are prerequisites for separating charge-transfer from non-charge-transfer states. Thus the bandwidth of the incident radiation and the ΔE of the electron analyser were both set to 100 meV.

Electronic structure calculations. The density functional calculation of the electronic structure of c(4 × 2)S/Ru(001) has been performed using the SIESTA code[24,25]. We used a symmetric slab containing 7 Ru layers and the surface geometry known from LEED[21,22]. Approximately 5 eV below the Fermi energy a strong S $3p$ density of states is found. Above the Fermi level we also find a broad resonance with a large weight on the S $3p$ orbitals, although strongly hybridized with Ru states in an anti-bonding S–Ru interaction. The resonance maximum lies ~2 eV above the Fermi level, which is marginally higher than the experimentally observed resonance maximum at 1.68 ± 0.1 eV above the Fermi level.

Calculation of the charge transfer times. The charge transfer dynamics are computed using the electronic hamiltonian obtained in the density functional calculations previously described. The initial electron wave packet $|\phi_R>$ is constructed as a projection of a linear combination of the S $3p$ orbitals onto the unoccupied bands at the energies of the resonance region. The wavefunction of the resonance depends on the excitation process. Since the electron is excited from a state of s-symmetry, the admixture of p_x,p_y and p_z components is given by the direction of the electric field vector of the incoming radiation **E**. Therefore we take $|\phi_R> = |\phi(t=0)> \propto \sum_i E_i |p_i>$. From the time evolution of the wave packet we can calculate the probability of finding the electron in the initial state $P(t) = |A(t)|^2$, where $A(t) = <\phi_R|\phi(t)>$ is the so-called survival amplitude. The Fourier transform $A(t)$ is directly related to the projection of the Green function onto the initial state $\tilde{A}(\omega) \propto <\phi_R|\hat{G}(\omega)|\phi_R> = G_{RR}(\omega)$ (ref. 26). The characteristic decay time of the resonance population τ is then computed using two procedures. Either the width of the resonance Δ is directly estimated from $G_{RR}(\omega)$ and $\tau = \hbar\Delta^{-1}$, or $P(t)$ is transformed into real time and τ is defined such that $P(t) \leq 1/e$ if $t \geq \tau$. Both methods produce very similar results. However, we prefer the second method since τ is obtained directly and it is not necessary to assume the lorentzian line-shape. We should point out that $G_{RR}(\omega)$ has to be calculated for the semi-infinite system, that is, we have to get rid of the finite size effects associated with the slab calculations. This is instrumental in getting reliable resonance widths and lifetimes. This is done by combining the information from a slab calculation with the *ab initio* hamiltonian obtained for bulk Ru and using recursive techniques to calculate$G_{RR}(\omega)$. We have assigned an error bar of 0.15 fs to our theoretical values. This reflects both the presence of two non-equivalent sulphur atoms in the surface and the numerical accuracy of our procedure.

Received 18 January; accepted 20 May 2005.

1. Zewail, A. H. Femtochemistry: atomic-scale dynamics of the chemical bond (adapted from the Nobel lecture). *J. Phys. Chem. A* **104,** 5660–5694 (2000).
2. Hentschel, M. *et al.* Attosecond metrology. *Nature* **414,** 509–513 (2001).
3. Drescher, M. *et al.* Time-resolved atomic inner-shell spectroscopy. *Nature* **419,** 803–807 (2002).
4. Baltuska, A. *et al.* Attosecond control of electronic processes by intense light fields. *Nature* **421,** 611–625 (2003).
5. Steinmeyer, G., Sutter, D. H., Gallmann, L., Matuschek, N. & Keller, U. Frontiers in ultrashort pulse generation: Pushing the limits in linear and nonlinear optics. *Science* **286,** 1507–1512 (1999).
6. Petek, H. & Ogawa, S. Femtosecond time-resolved two-photon photoemission studies of electron dynamics in metals. *Prog. Surf. Sci.* **56,** 239–310 (1997).
7. Kienberger, R. *et al.* Atomic transient recorder. *Nature* **427,** 817–821 (2004).
8. Goulielmakis, E. *et al.* Direct measurement of light waves. *Science* **305,** 1267–1269 (2004).
9. Björneholm, O., Nilsson, A., Sandell, A., Hernnäs, B. & Martensson, N. Determination of time scales for charge-transfer screening in physisorbed molecules. *Phys. Rev. Lett.* **68,** 1892–1895 (1992).
10. Ohno, M. Deexcitation processes in adsorbates. *Phys. Rev. B* **50,** 2566–2575 (1994).
11. Björneholm, O. *et al.* Femtosecond dissociation of core-excited HCl monitored by frequency detuning. *Phys. Rev. Lett.* **79,** 3150–3153 (1997).
12. Keller, C. *et al.* Ultrafast charge transfer times of chemisorbed species from Auger resonant Raman studies. *Phys. Rev. Lett.* **80,** 1774–1777 (1998).
13. Keller, C. *et al.* Femtosecond dynamics of adsorbate charge-transfer processes as probed by high-resolution core-level spectroscopy. *Phys. Rev. B* **57,** 11951–11954 (1998).
14. Feifel, R. *et al.* Observation of a continuum-continuum interference hole in ultrafast dissociating core-excited molecules. *Phys. Rev. Lett.* **85,** 3133–3136 (2000).
15. Wurth, W. & Menzel, D. Ultrafast electron dynamics at surfaces probed by resonant Auger spectroscopy. *Chem. Phys.* **251,** 141–149 (2000).
16. Brühwiler, P. A., Karis, O. & Mårtensson, N. Charge-transfer dynamics studied using resonant core spectroscopies. *Rev. Mod. Phys.* **74,** 703–740 (2002).
17. Schnadt, J. *et al.* Experimental evidence for sub-3-fs charge transfer from an aromatic adsorbate to a semiconductor. *Nature* **418,** 620–623 (2002).
18. Föhlisch, A. *et al.* Energy dependence of resonant charge transfer from adsorbates to metal substrates. *Chem. Phys.* **289,** 107–115 (2003).
19. Keller, C. *et al.* Electronic transfer processes studied at different time scales by selective resonant core hole excitation of adsorbed molecules. *Appl. Phys. A* **78,** 125–129 (2004).
20. Coville, M. & Thomas, T. D. Molecular effects on inner-shell lifetimes: Possible test of the one-center model of Auger decay. *Phys. Rev. A* **43,** 6053–6056 (1991).
21. Schwennicke, C., Jürgens, D., Held, G. & Pfnür, H. The structure of dense sulphur layers on Ru(0001) I. The c(2x4) structure. *Surf. Sci.* **316,** 81–91 (1994).
22. Jürgens, D., Schwennicke, C. & Pfnür, H. Surface structure analysis of the domain-wall phase of S/Ru(0001) using an efficient parameter optimization method. *Surf. Sci.* **381,** 174–189 (1997).
23. Krause, M. O. & Oliver, J. H. Natural widths of atomic K and L levels, K alpha X-ray lines and several KLL auger lines. *J. Phys. Chem. Ref. Data* **8,** 329–338 (1979).
24. Sánchez-Portal, D., Artacho, E., Ordejón, P. & Soler, J. M. Density-functional method for very large systems with LCAO basis sets. *Int. J. Quant. Chem.* **65,** 453–461 (1997).
25. Soler, J. M. *et al.* The SIESTA method for ab initio order-N materials simulation. *J. Phys. Condens. Matter* **14,** 2745–2779 (2002).
26. Borisov, A. G., Kazansky, A. K. & Gauyacq, J. P. Resonant charge transfer in ion–metal surface collisions: Effect of a projected band gap in the H-Cu(111) system. *Phys. Rev. B* **59,** 10935–10949 (1999).

Acknowledgements We acknowledge support by the staff of MAX-lab, Lund, Sweden, in particular J. N. Andersen and the ARI program. This work was supported by the Deutsche Forschungsgemeinschaft under Schwerpunktprogramm 1093 "Dynamik von Elektronentransferprozessen an Grenzflächen", the Basque Departamento de Educación, the University of the Basque Country, the Spanish MEC, European Network of Excellence NANOQUANTA, and Max-Planck Awards for Scientific Cooperation to P.M.E. and D.M.

Author Information Reprints and permissions information is available at npg.nature.com/reprintsandpermissions. The authors declare no competing financial interests. Correspondence and requests for materials should be addressed to W.W. (wilfried.wurth@desy.de).